We are IntechOpen, the world's leading publisher of Open Access books
Built by scientists, for scientists

6,900
Open access books available

186,000
International authors and editors

200M
Downloads

154
Countries delivered to

Our authors are among the
TOP 1%
most cited scientists

12.2%
Contributors from top 500 universities

CLARIVATE ANALYTICS
BOOK CITATION INDEX
INDEXED

WEB OF SCIENCE™

Selection of our books indexed in the Book Citation Index
in Web of Science™ Core Collection (BKCI)

Interested in publishing with us?
Contact book.department@intechopen.com

Numbers displayed above are based on latest data collected.
For more information visit www.intechopen.com

Interferometry to Detect Planets Outside Our Solar System

Marija Strojnik and Gonzalo Paez
Centro de Investigaciones en Optica
Mexico

1. Introduction

Humanity has been interested in exploring its environment since earliest historical times. After traveling across oceans using star navigation (Scholl, 1993), we turned our attention to getting to know the planets inside our Solar system (Arnold et al., 2010). After they were visited at least once with robotic vehicles (Scholl & Eberlein, 1993) or with an orbiting satellite, we asked ourselves whether conditions existed on any other planet for some form of life. It has been reported that nearly 500 planets were discovered with indirect methods: (a) passage of a dark planet in front of the bright solar disc (Brown et al., 2001); (b) movement of the center of gravity of a two-body system and Doppler shift (Butler et al., 2001); (c) Gravitational bending of rays passing a solar system larger than due to only star (Udalski et al, 2005); (d) using spectroscopy (Richardson, 2007); and (e) astrometry, to list a few. Initial research findings include dust clouds and double stars with different sizes (Moutou et al, 2011; Wright et al., 2001).

We rely principally on the visual system to receive the information about our environment. Such information is carried by the electromagnetic radiation. For a standard observer the visual spectral width covers only from about 0.38 μm to about 0.78 μm (1 μm =10^{-6} m, according to the MKS units employed in this paper) (Strojnik & Paez, 2001). Scientists have developed detectors to cover the electromagnetic spectrum from neutrinos and x-rays to radio waves. We use the word optical to cover visible and infrared (IR). Long-wave IR smoothly transitions into the sub-millimeter range. Many scientists differentiate between them upon incorporation of distinct detecting schemes. When a bolometer may be incorporated, the IR techniques are recognized (Artamkin et al., 2006; Khokhlov et al., 2009; Maxey et al., 1997). When the need arises for a local oscillator, millimeter terminology becomes dominant (Hoogeveen et al., 2003; Kellsall et al., 1993; Wirtz et al., 2003). The planet detection techniques that employ the "light", or the electromagnetic radiation, to detect the planet are generally considered the direct techniques.

2. Planet detection problem

The planet detection challenges have been formulated based on the radiometric, distance, and technology issues as a signal detection problem, under very unfavorable conditions (Scholl, 1994a, 1995, 1996a). The issues are best understood with the reference to Fig. 1. We would like to find a simplest solar system defined as having one star, similar or identical to

our Sun, and one planet, likewise similar or identical to out biggest planet, Jupiter. We propose to refer to such a star as the Estrella, and its planet the Tierra, because any of the nearby stars that already have a name may also have an invisible companion. This avoids confusion with our star and our planet(s). Our Sun radiates as a blackbody emitter at 5 800 K. The temperature of our largest and most distant planet, Jupiter, is estimated at 125 K.
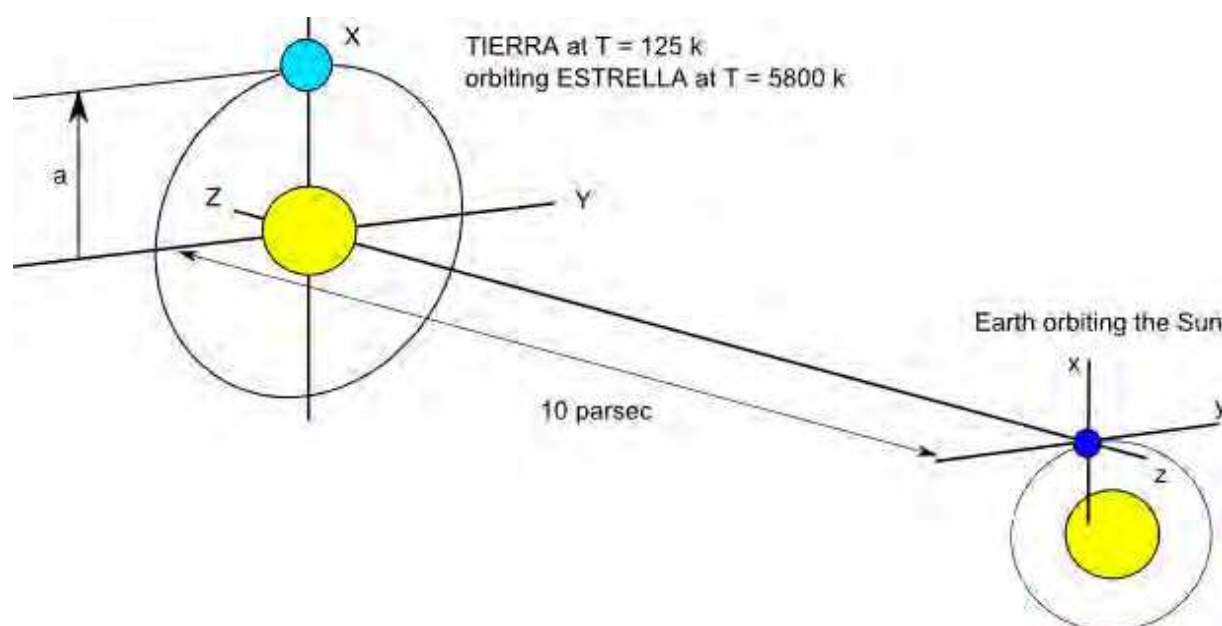

Fig. 1. Geometry for the detection of a planet outside our Solar system. The Earth-/ interferometer-based coordinate system is given as a Cartesian system (x,y,z), while the nearby Planetary system is displaced along the optical axis, Z-axis, with the Cartesian coordinates (X, Y, Z).

Such a planet is considered to be easiest to detect because of its large distance from the Sun. Thus, Figure 1 depicts the Tierra at its most favorable configuration for detection. The probability that the Tierra orbits the Estrella in a plane normal to the line of sight between the Estrella and the Earth, with its observing instrument, is rather small. However, at one particular moment of time, corresponding to the initial observation, the Tierra will be at a projected distance *a* from the Estrella. Its orbit may follow an elliptical path when projected on the plane normal to the line connecting the Estrella and The Earth. Tierra's local year determines the rotational period when the Tierra completes one orbit around the Estrella. In this simplest model, it would be equal to that of Jupiter and appreciably longer than 365 Earth days, let us say twice as long.

Our Solar system is located in the part of the universe where there are only a few Sun-like stars. Figure 2 displays the number of potential Estrellas as a function of stellar magnitude, m_v. This is defined as the star brightness relative to that of a reference star, in a logarithmic scale. In this scale, the Sun's stellar magnitude is 4.8. The astronomers assure us that the number of the stars in the universe is infinite. We concentrate on the stars within a sphere of a certain radius with the origin at the Earth. Restricting ourselves to the Sun-like stars, we find that there are only two such stars within 5 parsecs from us. One parsec is 3.26 light years, or it is the distance that a photon transverses when it travels in a straight line for 3.26 years. So, the distance in metric units is equal to $[(3 \times 10^8$ m/sec) x (3.26 years x 365

days/year x 24 hr/day x 60 min/hr x 60 sec)], a very large number, without much meaning for a mere human. There are about ten stars with the stellar magnitude equal to that of Sun within the distance of ten parsecs. When a sixteen-year old youth looks at fifteen nearby stars at night, the photon that is incident on his retina has left the star when the teenager was born. The number of potential Estrellas increases with the stellar magnitude and their distance from our Solar system.
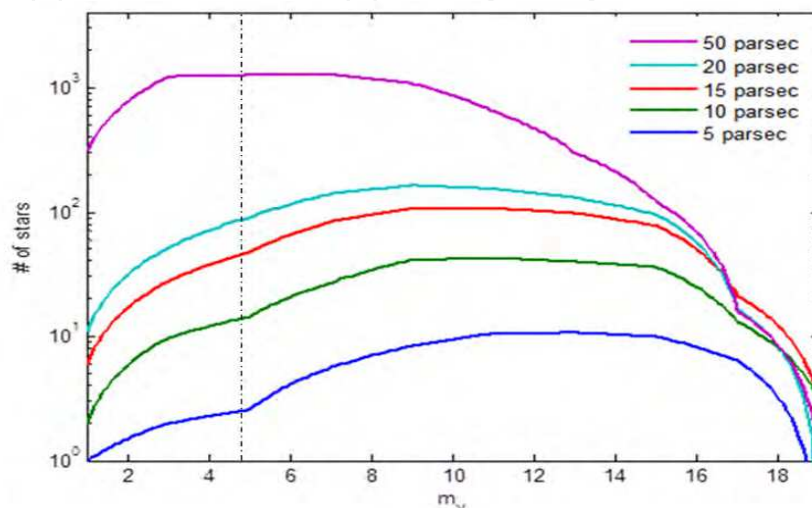

Fig. 2. Number of stars in the vicinity of Sun as a function of stellar magnitude, with the distance from the Sun as a parameter. The Sun's magnitude of 4.8 is indicated with a vertical line. The number of stars roughly increases with the stellar magnitude and the distance from the Sun. Calculated using star catalogues (Smithsonian Astrophysical Observatory, Telescope Data Center, 1991; The Yale Bright Star Catalog, 5th revised ed., Available at http://tdc-www.harvard.edu/catalogs/bsc5.html [accessed 10/22 2011]; CASU astronomical data centre, 2006; The Hipparcos, available at http://archive.ast.cam.ac.uk/hipp/hipparcos.html, [accessed 10/22/2011]; NASA's High Energy Astrophysics Science Archive Research Center, 2011; Gliese Catalog of nearby Stars, Available at http://heasarc.gsfc.nasa.gov/W3Browse/star-catalog/cns3.html; [accessed 10/22/2011]; NASA's Astrobiology Magazine, 2007; Catalog of Nearby Habitable Stars; available at http: //www.nasa.gov/vision/universe/newworlds/HabStars.html, [accessed 10/22/ 2011]).

Looking at the stars from the Earth, we can make three observations. Stars are very bright; they are far away; and they look like point sources to human observers and to any optical instrument, either constructed or under consideration at this time.

We apply the principle of the reversibility to the emitting and intercepting apertures in the power transfer equation to appreciate the signal collection (Strojnik & Paez, 2001). We imagine that sources are planets in our Solar system, with radiation intercepted with an aperture at a distant Tierra. Figure 3 illustrates the engineering and technological issues associated with the darkness of the planets. It graphs the number of spectral photons as a function of wavelength emitted by some representative planets in our Solar system intercepted by a unit aperture at a distance of 10 parsecs. The Earth surface is modeled to emit as a blackbody at the average temperature of 300 K, while the Jupiter temperature is assumed at 125 K. Kelvin (1 K) is a unit of temperature with the same magnitude as 1 C (centigrade or Celsius scale), but with its zero at -273.13 C, considered the absolute zero for temperature.

We observe that the intercepting aperture at the Tierra at a distance of 10 parsecs collects one photon at 34 μm per second originating at Jupiter, and about 70 photons at 12 μm from the Earth. Solely on the basis of the low levels of light emission, large integration times on the order of hours are needed for the collection of the requisite signal. This leads into the stringent requirement for a stable platform on which the planet-detecting system is to be mounted.
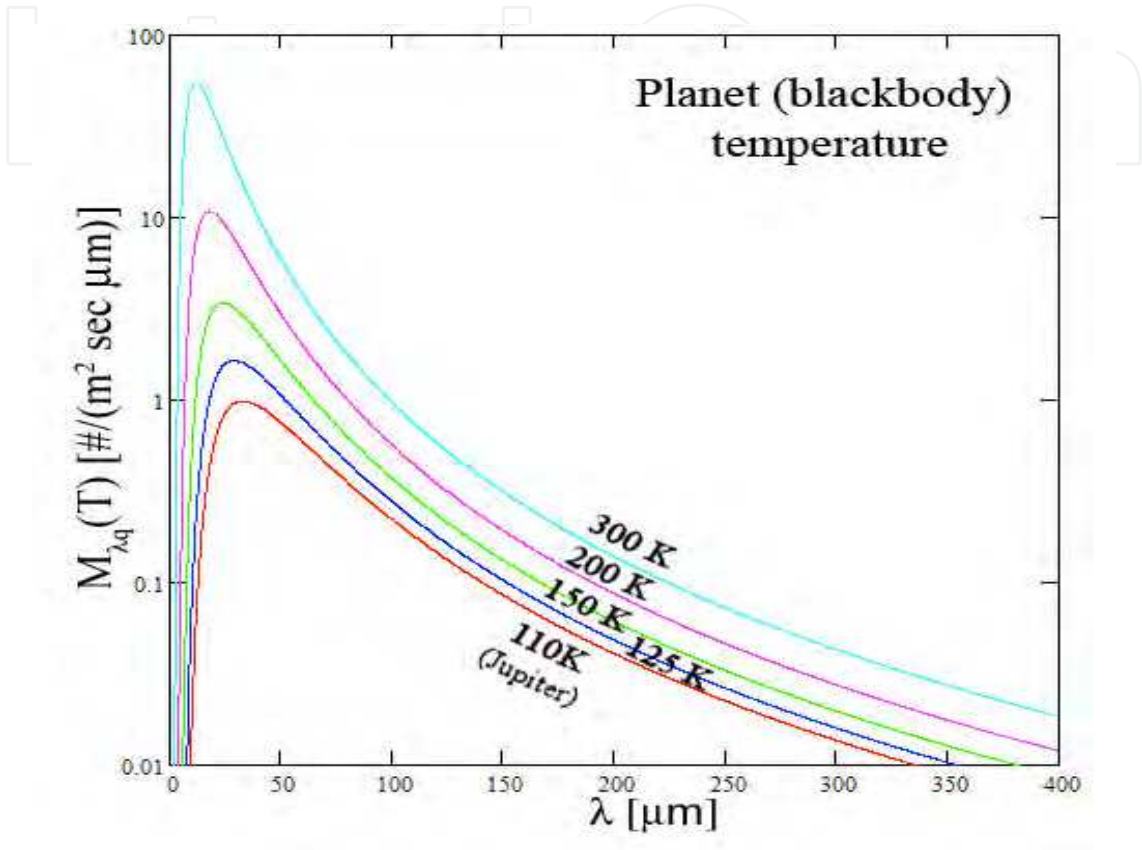

Fig. 3. Number of spectral photons emitted as blackbody radiators due to their surface temperature, per unit time and unit area, by several representative planets in our Solar system, intercepted at a distance of 10 parsec by a unit aperture (1 m²), versus wavelength.

Comparing the emission of our planets to that of our Sun, we can draw some additional conclusions. Planets emit much less radiation than the Sun and they are much smaller. These considerations translate into three significant optical problems. We address the radiometric problem first.

2.1 Faint planet near the bright star: radiometric problem

Most detectors, including human eye, have a great deal of difficulty detecting a very bright and a very dim object at the same time. The limits in the dynamic range, saturation, and "bleeding" of the bright object onto the image of the dim object prevent their simultaneous detection. Figure 4 depicts the radiometric problem illustrating the darkness of the planets relative to the brightness of the Sun by looking at some representative planets in our Solar system. It graphs the ratio of the number of spectral photons emitted by several representa-tive planets divided by the number of spectral photons emitted by the Sun, at its peak

emission, as a function of wavelength. In this analysis, two sources of emission are considered for the planets: self emission due to the planet surface temperature and the radiation originated at the Sun, intercepted by the planet and reflected from it. For us, the Sun and the planets are considered extended bodies; therefore, the distant and large Jupiter reflects about ten times the amount of radiation at 0.7 µm than the Earth. Planet Uranus is distant and small, subtending a relatively small solid angle at the Sun and reflecting nearly a hundred times less Sun radiation at the peak of the Sun emission than the Earth.
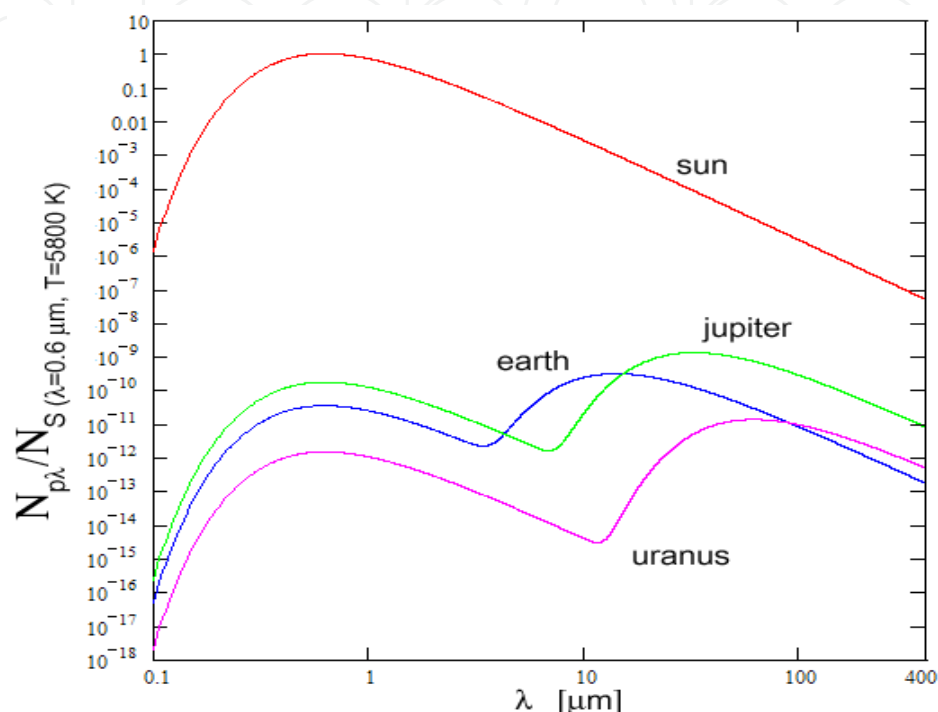

Fig. 4. Number of spectral photons emitted by the Sun and several planets as a function of wavelength, normalized against solar emission at Sun's maximum emission wavelength. The ratio of the number of planet spectral photons over the number of Sun's spectral photons is defined as the simplest signal-to-noise ratio.

In Fig. 4, the Tierra distance is not important, because it is normalized. Both the planet and the Sun are treated as point sources, and both are observed from the same large distance. The size of the intercepting area and signal collection time are the same for both Sun and its planet. The Sun emission curve is normalized to 1 at its peak emission as a blackbody radiator at temperature of 5 800 K. See (Strojnik & Paez, 2001) for blackbody emitters.

This is basically the simplest spectral radiometric signal-to-noise ratio, considered in most publications dealing with the Tierra detection. The signal is defined as the quantity of interest, i.e., the number of photons originating at the planet. The radiation emitted by the Estrella is thus considered noise. Other sources of noise may be considered when the instrumental concept starts to take a more definite form in the quest for the Tierra detection.

The analysis displays the spectral information, i.e., the number of (spectral) photons as a function of wavelength, because all the detectors have a limited detection interval. They will detect all radiation incident on its sensitive surface, independently of its origin, dependent

only on its spectral sensitivity. This means that no photon absorbed by the detector sensitive surface is labeled as "coming from a planet" or any other object.

We next examine some potential detection wavelength bands. At the peak Sun emission in the visible, the number of Sun photons reflected from the Jupiter is by the factor of 10^{-10} smaller than the number directly emitted by the Sun. This may be read directly from the vertical coordinate in Fig. 4. The signal-to-noise ratio is nearly ten times smaller still for the Earth, decreasing nearly to 10^{-11}. This value arises purely from the planet diameter and distance from the Sun. Self-emission is negligible at this wavelength region (see also Fig. 3).

Going to the longer wavelengths, we find the second peak due to the planetary self-emission, with the peak location determined by the planet temperature. It is also shifted due to the decreasing Sun emission at longer wavelengths. In the case of the Earth, the signal-to-noise peak for spectral photons is found to be 10^{-6} at about 18 μm. Examining the more favorable case of the Jupiter, we find the peak with spectral photon signal-to noise ratio of 10^{-4} at about 35 μm. Interestingly, though, this is not the peak signal-to-noise ratio. As the Sun emission falls off more rapidly than that of the Jupiter, the photon signal-to-noise ratio slowly increases with increasing wavelengths. At 100 μm it becomes about 3×10^{-4}. The rate of the photon signal-to-noise ratio increase, while relatively small, is about 2×10^{-2} μm^{-1}. We momentarily concentrate on even longer wavelengths, say around 300 μm, and we apply this rate of increase to the photon number ratio. We calculate it to be about 10^{-3} at 300 μm. Interestingly, this wavelength range corresponds to the spectral region where the Earth atmosphere becomes partially transmissive at elevated heights.

2.2 Faint planet next to a bright star: imaging problem

2.2.1 Coronagraphic Estrella signal elimination

When considering the issue of imaging an Estrella-Tierra object scenario, we momentarily set aside the concern that no star (with the exception of Sun) may be resolved at this time with any existing optical telescope or instrument. It is quite amazing that the author's original paper on the planet detection was rejected in the early 90s, because the reviewer considered detection at 18 μm something technologically impossible and therefore not worthy of being published. Today, about 20 years later, the detector technology is being developed at an ever-faster rate, covering increasingly longer wavelengths (Boeker et al., 1997; Farhoomand et al., 2006; Martijn et al., 2005, Müller et al., 2010; Olsen et al., 1997; Reichertz et al., 2005; Royer et al., 1997; Thomas et al., 1998; Young, 1993). Focal plane architectures are being implemented for cameras, some incorporating bolometers, for far IR / sub-mm spectral range (Agnese et al., 2002; Poglitsch et al., 1997; Wilson et al., 2004). This is exactly the spectral region where the photon signal-to-noise ratio has been shown to be most favorable in the previous section. Therefore, we anticipate that the technology exists to image the Estrella and the Tierra onto the same focal plane.

We here adhere to the geometry that the diameter of the Estrella is ten times the diameter of Tierra, the case of Jupiter, with the angular separation of 2 μrad for the observation distance of 10 parsecs. Under these conditions, the Estrella subtends 0.0002 micro-radians (2×10^{-4} μrad), and the Tierra ten times less, or 0.00002 micro-radians (2×10^{-5} μrad). The basic requirement to achieve imaging, by the definition of imaging, is that there be a disk detected

in the focal plane corresponding to the Estrella and another one corresponding to the Tierra, displaced by their huge angular separation. The disc diameters have a ratio of ten. With imaging strategy, we arbitrarily set the Estrella on the optical axis and the ten-times smaller planet at the edge of the field. Ideally, the image of the planet falls exactly on one detector (pixel) to optimize the planet detection. Considering that we are not interested in the Estrella, we may implement the inverse coronagraphic configuration in the first focal plane to pass the Estrella rays through the focal plane. The traditional coronagraphic configuration blocks the image of the Sun (Gordley et al., 2005; Scholl, 1993, 1996; Scholl & Paez, 1997b; Schultz et al., 1999; Suzuki et al., 1997).

Radiation blocking scheme might also produce a great amount of reflected and absorbed radiation that travels all over and causes stray-light noise (Scholl, 1994b; Stauder & Esplin, 1998) and heating. Such scattered radiation might easily drown the faint signal (Scholl, 1996b). The inverse coronagraphic configuration would let the Estrella rays pass through a hole in the focal plane, while detectors would be placed outside the opening. The relatively great angular separation between them would assure that only the Tierra signal is detected.

The major shortcoming of this elegant proposal is that there is no telescope currently under consideration that would allow imaging of a nearby solar system, or even a nearest star. The secondary concerns are the stray light issues, scattering, and the tremendous brightness differences between two objects in the same scene even if imaged in different image planes. All of these concerns are just the technological limitations that will be overcome with the passage of time. Next we examine the most critical one, that of imaging and resolution.

2.3 Small (point) planet next to a distant (point) star: resolution problem

The resolution is an attribute of an imaging system. It deals with the fact that an image of a point object is not a point, but rather a blob (Paez & Strojnik, 2001). Image of a point source obtained in the focal plane of an instrument spreads out due to diffraction, aberrations, fabrication errors, and misalignment. The spot size and shape depend on many additional factors, including mechanical stability of the platform and the electronic system for the control of motion. The image spread can never be completely eliminated (see left side of Fig. 5). The resolution of a moderately aberrated optical system is defined by the radius of the spot encircling 90% of energy (or rays) originating at a point source.

There are several resolution criteria, but the most common one deals with the imaging of two point sources of equal brightness/ (spectral) intensity separated by an angle θ. Brightness usually refers to the visual perception of a human. (Spectral) intensity is the (spectral) power emitted into the solid angle. According to the widely-accepted Rayleigh resolution criterion, two such point sources may be resolved under optimal conditions if their angular separation is $\theta = 1.22 \, \lambda/D$, where λ is the wavelength of the image forming radiation and D is the diameter of the aperture. The images of two point sources of equal intensity resolved according to the Rayleigh criterion are illustrated on the right side of Fig. 5.

For the largest IR telescope currently under construction (see Fig. 6a), the Great Millimeter Telescope GMT) being built in Mexico, the design wavelength is 1 mm, and the aperture diameter is 50 m, giving the angular resolution of about 2×10^{-5} rad, or 20 µrad. (For more information on the status of this observatory, please see its web address). This angle is ten times larger than the angular separation between the Estrella and the Tierra at
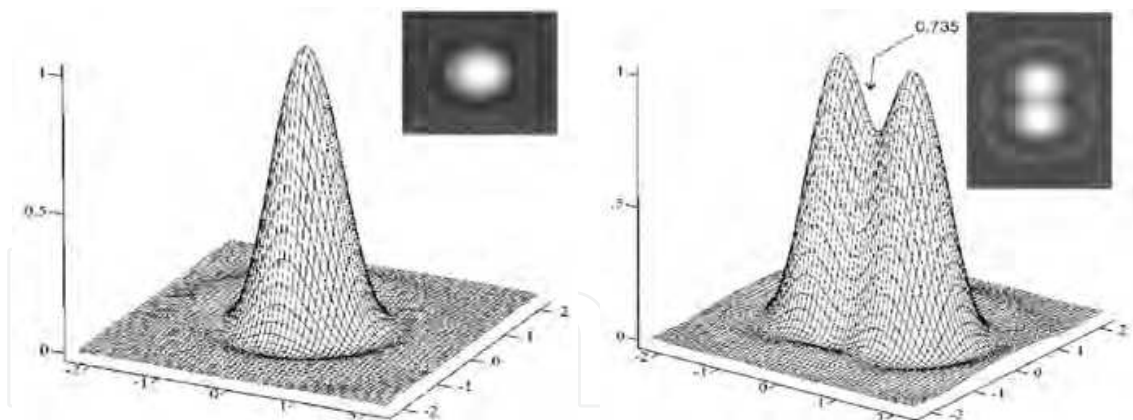
Fig. 5. Left: image of a point source obtained in the focal plane of an instrument spreads out due to diffraction, aberrations, fabrication errors, and misalignment. Right: images of two point sources of equal spectral intensity resolved according to the Rayleigh criterion.

10 parsecs. However, the construction of this telescope has been progressing with better achievements than the original design prediction, laying grounds for the confidence that the telescope will perform well down to 0.1 mm or 100 μm. At this wavelength, the image of the bright point source, the Estrella, will have its zero at 2 μrad, or at the estimated Tierra angular position, θ_{TC}. Likewise, the image of the Tierra will peak at 2 μrad and have its zero on the optical axis. If the Estrella and the Tierra had the same intensity, i. e., if they formed a double star, their image obtained by the GMT at 0.1 mm would be similar to that in Fig. 5b. Due to the spectral intensity ratio between the Estrella and the Tierra (about 10^3 at 300 μm) their image would look a lot like Fig. 5a. The bright spec on the dark ring would be seen possibly in the logarithmic rendition, and would easily be confused with noise.

It is nothing more than a fortunate coincidence that straw-man design parameters, proposed in the nineties, correspond to the desirable features of the GTM telescope under construction. However, the tentative Planetary system parameters do not necessarily correspond to the characteristics of an actual solar system.

2.4 Earth and space based telescopes

2.4.1 Space- and air-borne telescopes

Some of the issues dealing with the telescopes have been summarized in the literature (Paez & Strojnik, 2001). The air turbulence, sometimes referred to as "seeing", and spectral transmission of the atmosphere limit the usefulness of large-diameter monolithic or phased telescopes on the Earth surface. The water in the atmosphere attenuates the transmission of the IR radiation so most IR telescopes perform best in space. (Hofferbert et al., 2003; Kessler & Harvit, 1993; Lamarre, 1993; Lemke et al., 2005; Mather, 1993; Matsumoto & Murakami, 1996; Scholl & Paez, 1997a; Touahri et al., 2010). The great disadvantage of the space-based IR telescopes is that their instruments require cooling, often to liquid Helium temperatures (Beeman & Haller, 2002; Latvakoski et al, 2010). The supply of the coolant basically limits the useful life of the IR space observatory, telescope and on-board instruments. The instruments that are cooled to higher temperatures function longer and collect the scientific data for longer period of time (Schick & Bell, 1997).
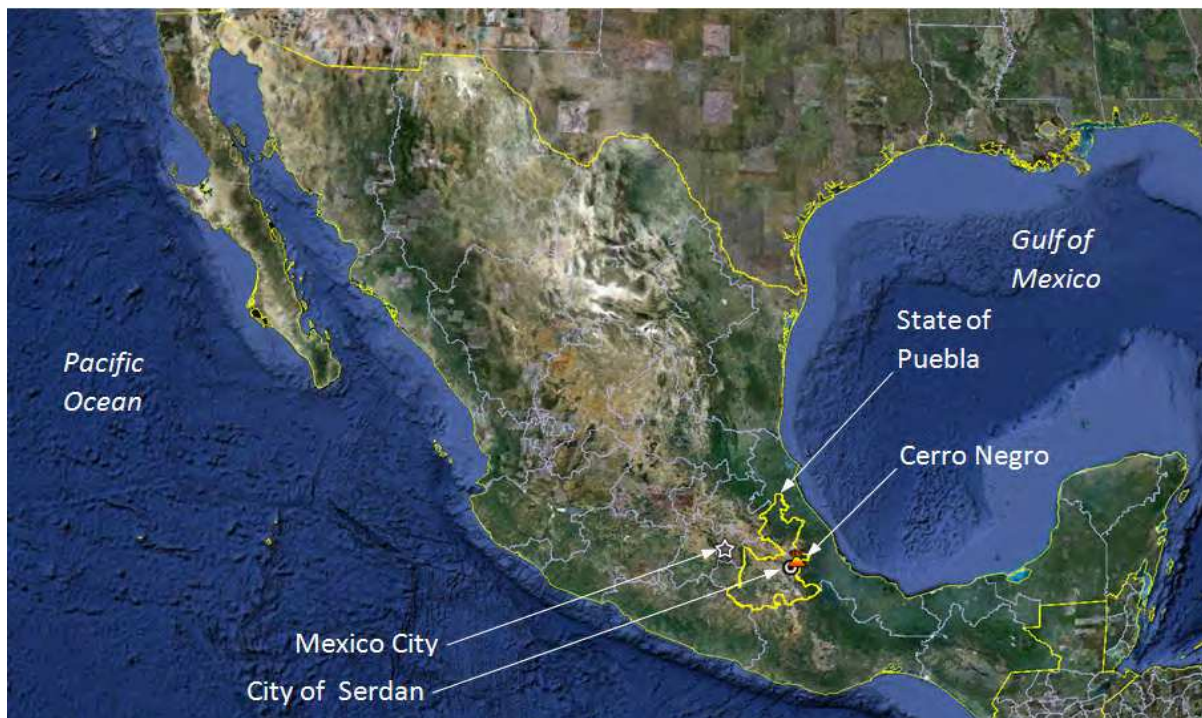
Fig. 6a. The GMT facility's location in the Mexican state of Puebla, on top of a high mountain, between the Atlantic Ocean / the Gulf of Mexico (E) and the Pacific Ocean (W).

This limitation of the lifetime of the satellites has given rise to a new observational facility type, balloon-borne instruments (Catanzaro et al., 2002), rocketborne instruments (Elwell, 1993), and jet-carried observatory. SOFIA (Stratospheric Observatory for IR Astronomy) has a telescope built inside a modified 747P jet to fly in the stratosphere (Becklin & Gehrz, 2009; Krabbe, & Casey, 2002; updated information is available on the web). It incorporates a 2.5 m aperture, flying at the height of about 14 000 m. The telescope looks sideways through the thinned atmosphere at the IR sky. The airplane can land after exhausting its fuel supply, resupply the coolant for the telescope, its instruments, and focal planes; and change the instruments. The most demanding requirement facing the observatory in an airplane is the stability of the aircraft, especially for the long detector-integration times needed for the observation of faint objects.

2.4.2 Transmission of the Earth atmosphere

Placing the observatory on a more solid base would solve the problem of stability. This could be achieved by placing it on the top of a very high mountain, depicted in Fig. 6a. Cerro Negro, Orizaba, Puebla (state), Mexico, where the GMT is being finished) is 4,600 m above the sea level. The significant problem of the absorption of the far IR radiation by water in the thinned atmosphere is ameliorated by dryness of the region, and specifically by a very small number of days characterized by high humidity. Even though Mexico borders on two oceans, Atlantic/ Golf of Mexico and Pacific, its land mass is enormous and characterized by dry heat. Puebla's significant distance from the coastlines and the observatory elevation assures dryness of the cold air above the observatory. Figure 6b presents actual photo of the telescope. In difference to the aircraft implementation, the celestial objects may be viewed in nadir.

Fig. 6b. The GMT (http://www.lmtgtm.org/images/sitepics05012011/LMTatSunrise1.jpg) observatory construction site, with the last ring of the antenna in the process of installation.

In the airplane, the IR radiation passes through the thinned atmosphere at 14,000 m with sufficient density to allow the plane to remain in the air. Due to the side opening for the telescope viewing, the radiation passes horizontally through several equivalent air masses to contribute an approximately equivalent amount of atmospheric scattering and absorption as the nadir-viewing telescope at 4,600 m (Wellard et al., 2006).

No data has yet been made available for the transmission at the far IR / sub-millimeter/ millimeter spectral region at The Cerro Negro in Mexico. There have been long-term measurements taken for a number of years at another millimetric facility at Chajnantor, in Chile, at the height of 5,100 m above sea level (Cageo et al., 2010). Figure 7 presents the graphs of the atmospheric transmission at this site, as a function of wavelength. This site is higher by 600 m, or about 11 % than that of the GMT.

We concentrate on the transmission peaks, referred to as band 10 in the Chilean telescope, from about 800 to 980 GHz. Due to our interest in the Tierra detection at about 300 μm (or about 900 GHz), where the photon number contrast achieves a highly favorable 0.001 signal-to-noise ratio, we examine the transmission band at about 900 GHz in more detail. Its transmission of radiation is about 0.4 when the atmosphere is dry. The transmission decreases by about 50 % in the case of the wet atmosphere. No such data has been reported for the GMT, but the great majority of days are dry. Independently of the amount of atmospheric absorption and scattering in this wavelength interval, the radiation attenuates equally for both the Estrella and the Tierra signal. Thus, the signal-to-noise ratio remains unchanged. We will use 0.4 as the working number for the transmission ratio for the site. Clearly, the data will be collected (or utilized) only under favorable observational conditions. Again, the smaller signal from the Tierra will be affected worse. Such detailed

considerations will be incorporated into the overall signal-to-noise ratio calculations, after the detection mechanisms and the instrument have been specified.
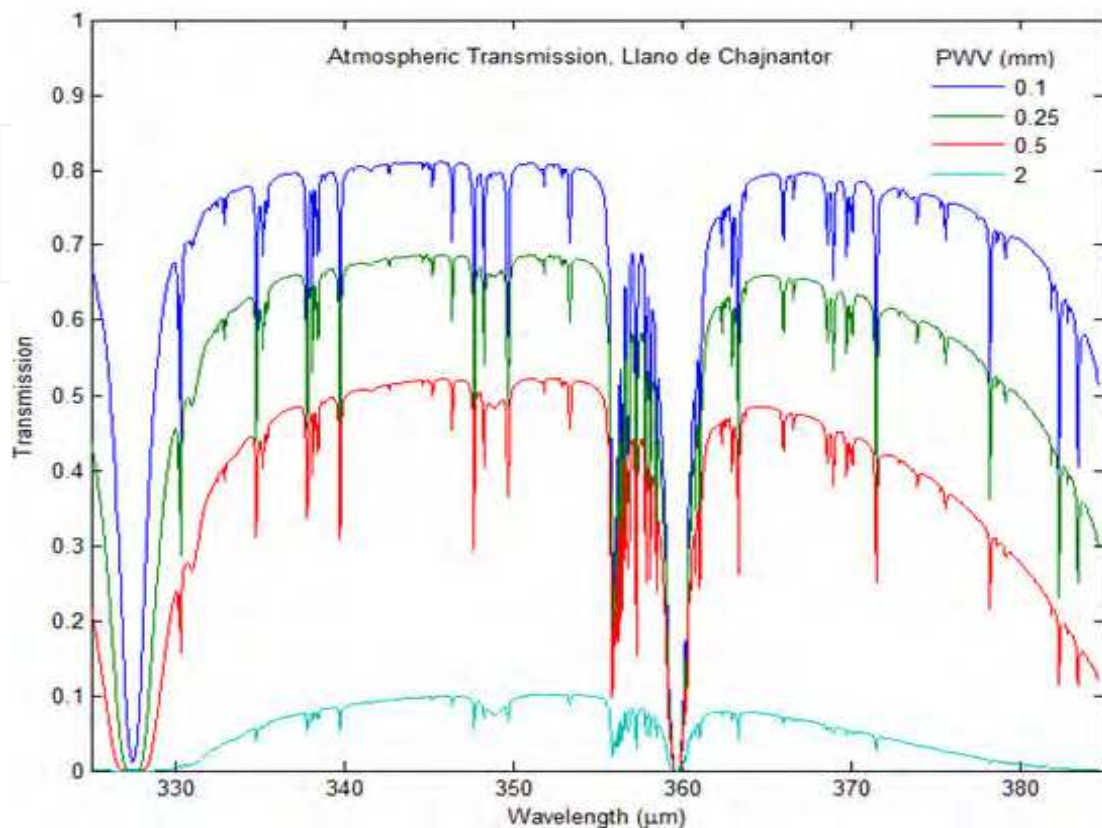

Fig. 7. Atmospheric transmission at the ALMA site on Llano de Chajnantor, Chile, at 5,100 m above the sea level, with the amount of precipitable water vapor as a parameter (after Atacama large millimeter/submillimeter array, https://almascience.nrao.edu /about-alma/weather/atmosphere-model [accessed 11/2/2011]).

3. Interferometry

3.1 Interferometer for the Tierra detection

3.1.1 Two-aperture interferometry

A panel of distinguished scientists proposed a two-aperture interferometer to detect the Tierra and null the Estrella (Bracewell, 1978). The basic idea was to use the interferometry to eliminate the radiation coming from the Estrella through the process of the destructive interference, while at the same time transmitting the radiation coming from the Tierra. In this concept the image of the Tierra would be located exactly on the dark interference fringe formed by the Estrella radiation. The scientists have not yet discovered the procedure of tagging the photons originating at the Tierra to send them through an image-forming instrument while allowing those from the Estrella to interfere destructively as necessary to implement this proposal. Thus, the radiation coming from both celestial sources through two apertures forms two interference patterns. The two patterns have the same period, but they are slightly displaced with respect to each other corresponding to the separation of the point sources in the plane of the Planetary system. This is the plane perpendicular to the line

of observation, or the optical axis. Their amplitudes have the same ratio as the simplest signal-to-noise ratio. Therefore, the Tierra modulation will be at least 10^3 times smaller than that of the Estrella. These two patterns overlap on the focal plane, with the visibility of the Tierra smaller by the signal-to-noise ratio in the interferometer plane (in the vicinity of Earth), by a factor of at least 10^3. The most important feature of either interference pattern is that its period is determined only by the aperture separation, also referred to as baseline (Strojnik & Paez, 2003; Vasquez-Jaccaud et al., 2010).

As the Tierra slowly rotates around the Estrella, the Estrella interference pattern remains unchanged relative to a stationary two-aperture interferometer. The displacement of the Tierra interference pattern approaches that of the Estrella as the Tierra's projection on the plane normal to the line-of-sight approaches the Estrella. When the Tierra is exactly in front of the Estrella, both on the Z-axis, the two interference patterns will be exactly in phase – the modulation of the combined pattern will be insignificantly smaller than that of the Estrella alone. When the Tierra is behind the Estrella, two-apertures produce the interferometric pattern due to the Estrella source independently whether the Estrella is accompanied by an orbiting Tierra or not. Thus, an interferometric pattern in a two-aperture interferometer does not confirm the existence of the Tierra.

3.1.2 Space interferometry

A large body of research and conceptual studies has been performed in support of these concepts, mostly for space applications. The need for the space system arises due to the opacity of the Earth atmosphere in many of the interesting regions. The most advanced developments were offered in the ESA studies, recently referred to as the Darwin proposal (most up-to date information is available on the Darwin web site). This free flying instrument would initially employ a multi-section telescope with a 5-m diameter. The study evolved to have two such telescopes connected into an interferometer with a precisely controlled baseline. It culminated in a proposal for a number of such telescopes that could be used as a sparsely-filled aperture to detect several spatial frequencies. The spatial frequency is defined as the number of lines per unit distance.

While the interferometric concepts assume detection of fringes from two different sources (detection of a single spatial frequency), the imaging concepts incorporate finding a significant number of key spatial frequencies. The incorporation of the sparsely-filled aperture implies that a number of spatial frequencies present in the object are missing in the image. As discussed in the imaging section, this would require rigid control of aperture separations, at distances of at least 50 meters to meet the Rayleigh resolution criterion for the Estrella and the Tierra at 10 parsecs. This separation would have to be increased even more to decrease the background diffracted and scattered radiation from the Estrella to a value comparable to that of the Tierra (for example, 10^{-3} at 300 μm). For the diffracted radiation from the Estrella to be less than the signal from the Tierra (under optimal observational conditions), two neighboring apertures might have to be separated by at least four times more than the resolution distance of 50 m, or 200 m. This considers only the diffraction effects of the apertures. To decrease the effects of gravity, this instrument would be placed at the first or the second Lagrangian point (zero gravity point between Earth and Moon). The ESA study has been temporarily set aside at the time of this writing, in favor of more

promising surveys of infrared and submillimeter skies, with Herschel and SPICA instruments, and the ESO Planck Observatory (more update information is available on the ESA Planck, AKARI web sites).

Many research studies continue to decrease the amount of the Estrella radiation in the detector plane, most of them quite interesting from the point of view of signal camouflaging and encoding. They are extensively discussed in the literature as a technique referred to as "nulling" of the star light.

Infinitesimally thin and infinitely long apertures help to conceptualize difficult problems, such as the Estrella being thought of as a point object. Such a case was treated rigorously, including both the interference and diffraction at finite apertures (Strojnik & Paez, 2003).

3.2 Transformation of a spherical wave into a plane wave upon propagation over large distances

We consider that the point on the Planetary system plane (either the point on the Estrella or on the Tierra) radiates as a point source. It is located at a distance r_{PS} from the plane of the aperture (of diameter D in meters), centered on the x, y plane. Due to the great distance of propagation, we consider the radiation incident on the plane of the apertures as coherent as proved in the Van Cittert-Zernike theorem. The distance r_{PS} (for Planetary system, with the subscript becoming E for the Estrella or T for the Tierra, as appropriate) may be written as follows. We refer to Fig. 1.

$$r_{PS}(x,y,z;X,Y,Z) = \sqrt{(X_{PS} - x)^2 + (Y_{PS} - y)^2 + (Z_{PS} - z)^2} \qquad (1)$$

Therefore, the point source in the planetary system plane radiates in all directions as a spherical wave with intensity $U_{PS}U_{PS}^*$.

$$U_{PS}(x,y,z;X,Y,Z) = U_{PS0}\left(\frac{e^{ikr_{PS}}}{r_{PS}}\right) \qquad (2)$$

We now make a few simplifying assumptions, considering that the Estrella-Tierra coordinate system is extremely far away. Then we expand r_{PS} in the exponent somewhat more carefully because the sine and cosine vary much more rapidly with their argument. We rewrite Eq. (2), factoring out z_{PS}, the distance on the optical axis between the planetary system and the interferometer plane. This quantity is significantly larger than other quantities in Eq. (1), according to the geometry of Fig. 1.

$$r_{PS}(x,y,z;X,Y,Z) = Z_{PS}\sqrt{\left[\left(1 - \frac{z}{Z_{PS}}\right)^2 + \left(\frac{X_{PS}}{Z_{PS}} - \frac{x}{Z_{PS}}\right)^2 + \left(\frac{Y_{PS}}{Z_{PS}} - \frac{y}{Z_{PS}}\right)^2\right]} \qquad (3)$$

We then square the expressions in the parentheses. The spatial extend of the Estrella is much, much larger than the lateral extend of the largest interferometer diameter considered in the current studies. We will neglect the square of the interferometer coordinates x, y, in comparison with $X_E x$ and $Y_E y$, respectively. We similarly assume that the separation of Tierra from the Estrella is much, much larger than interferometer extend.

$$r_{PS}(x,y,z;X,Y,Z) = Z_{PS}\sqrt{\left\{\begin{array}{l}\left[1-2\left(\dfrac{z}{Z_{PS}}\right)+\left(\dfrac{z}{Z_{PS}}\right)^2\right]\\[2mm] +\left[\left(\dfrac{X_{PS}}{Z_{PS}}\right)^2 -2\left(\dfrac{X_{PS}}{Z_{PS}}\right)\left(\dfrac{x}{Z_{PS}}\right)+\left(\dfrac{x}{Z_{PS}}\right)^2\right]\\[2mm] +\left[\left(\dfrac{Y_{PS}}{Z_{PS}}\right)^2 -2\left(\dfrac{Y_{PS}}{Z_{PS}}\right)\left(\dfrac{y}{Z_{PS}}\right)+\left(\dfrac{y}{Z_{PS}}\right)^2\right]\end{array}\right\}}$$ (4)

Therefore, we neglect the square of the interferometer coordinates x, and y, in comparison with the product $X_T x$ and $Y_T y$, respectively. In practice the telescope will be bore-sighted on the easily observable Estrella. We are keeping only the lowest order in x, y and z coordinates.

$$r_{PS}(x,y,z;X,Y,Z) = Z_{PS}\sqrt{\left\{\left[1+\left(\dfrac{X_{PS}}{Z_{PS}}\right)^2+\left(\dfrac{Y_{PS}}{Z_{PS}}\right)^2\right]-2\left[\left(\dfrac{z}{Z_{PS}}\right)+\left(\dfrac{X_{PS}}{Z_{PS}}\right)\left(\dfrac{x}{Z_{PS}}\right)+\left(\dfrac{Y_{PS}}{Z_{PS}}\right)\left(\dfrac{y}{Z_{PS}}\right)\right]\right\}}$$ (5)

We choose the plane of the aperture system at z = 0, or normal to the line of sight Plenary system – interferometer system. The first term in the second square bracket is equal to zero.

$$r_{PS}(x,y,z;X,Y,Z) = Z_{PS}\sqrt{\left\{\left[1+\left(\dfrac{X_{PS}}{Z_{PS}}\right)^2+\left(\dfrac{Y_{PS}}{Z_{PS}}\right)^2\right]-2\left[\left(\dfrac{X_{PS}}{Z_{PS}}\right)\left(\dfrac{x}{Z_{PS}}\right)+\left(\dfrac{Y_{PS}}{Z_{PS}}\right)\left(\dfrac{y}{Z_{PS}}\right)\right]\right\}}$$ (6)

Next we expand the square root, considering that the furthest transverse coordinate in the interferometer system is significantly smaller than the separation between the Planetary system and the interferometer. Likewise, the furthest transverse coordinate in the Planetary system is significantly smaller than the separation between the Planetary system and the interferometer. Thus the argument under the square root sign is 1 plus a small number. The expansion is valid when ε is much smaller than 1, with accuracy increasing when ε approaches to zero.

$$(1+\varepsilon)^m = 1+m\varepsilon$$ (7)

Using this expansion, Eq. (6) becomes.

$$r_{PS}(x,y,z;X,Y,Z) = Z_{PS}\left\{1+\left(\dfrac{1}{2}\right)\left[\left(\dfrac{X_{PS}}{Z_{PS}}\right)^2+\left(\dfrac{Y_{PS}}{Z_{PS}}\right)^2\right]-\left[\left(\dfrac{X_{PS}}{Z_{PS}}\right)\left(\dfrac{x}{Z_{PS}}\right)+\left(\dfrac{Y_{PS}}{Z_{PS}}\right)\left(\dfrac{y}{Z_{PS}}\right)\right]\right\}$$ (8)

The first two terms include only the coordinates associated with the objects on the Estrella-Tierra Planetary system. The second term includes both the planetary and interferometer coordinates. We let x and y be equal to zero, effectively choosing the point on the origin of the interferometer coordinate system. We may use the same expansion in Eq. (7) in reverse, and apply it to the first two terms (those dealing with the planetary system quantities.)

$$r_{PS}(X_{PS},Y_{PS},Z_{PS}) = r_{PS}(0,0,0;X_{PS},Y_{PS},Z_{PS})$$
$$= Z_{PS}\left\{1+\left(\dfrac{1}{2}\right)\left[\left(\dfrac{X_{PS}}{Z_{PS}}\right)^2+\left(\dfrac{Y_{PS}}{Z_{PS}}\right)^2\right]\right\} = Z_{PS}\sqrt{\left[1+\left(\dfrac{X_{PS}}{Z_{PS}}\right)^2+\left(\dfrac{Y_{PS}}{Z_{PS}}\right)^2\right]}$$ (9)

We substitute Eq. (9) into Eq. (8), to find an interesting result: we can separate the coordinates in the planetary system from the cross terms that include also those in the interferometer plane.

$$r_{PS}(x,y,z;X,Y,Z) = r_{PS}(X_{PS},Y_{PS},Z_{PS}) - Z_{PS}\left[\left(\frac{X_{PS}}{Z_{PS}}\right)\left(\frac{x}{Z_{PS}}\right)+\left(\frac{Y_{PS}}{Z_{PS}}\right)\left(\frac{y}{Z_{PS}}\right)\right] \tag{10}$$

Thus, we developed an expression for the value of r_{PS} to be inserted into the exponent of Eq. (2). We substitute Eq. (10) into Eq. (2).

$$U_{PS}(x,y,z;X,Y,Z) = U_{PS0}(X_{PS},Y_{PS},Z_{PS})\left\{\frac{e^{ik\left\{r_{PS}(X_{PS},Y_{PS},Z_{PS})-Z_{PS}\left[\left(\frac{X_{PS}}{Z_{PS}}\right)\left(\frac{x}{Z_{PS}}\right)+\left(\frac{Y_{PS}}{Z_{PS}}\right)\left(\frac{y}{Z_{PS}}\right)\right]\right\}}}{r_{PS}(X_{PS},Y_{PS},Z_{PS})}\right\} \tag{11}$$

The coordinates in the first term in the exponent X_{PS}, Y_{PS}, and Z_{PS} in Eq. (11) may only assume the values corresponding to a point within the spatial extent of the plenary system encompassing the Estrella and the Tierra. So, we factor it out and combine it into a single term for the amplitude that only depends on the coordinates of a point on the planetary system, X_{PS}, Y_{PS}, Z_{PS}. We next take advantage of the rules of multiplication of the exponentials, $\{\exp(a+b) = [\exp(a)][\exp(b)]\}$.

$$u_{PS}(x,y,z;X,Y,Z)$$
$$= \left\{U_{PS0}(X_{PS},Y_{PS},Z_{PS})\left[\frac{\exp[ikr_{PS}(X_{PS},Y_{PS},Z_{PS})]}{r_{PS}(X_{PS},Y_{PS},Z_{PS})}\right]\right\}\exp\left\{-ikZ_{PS}\left[\left(\frac{X_{PS}}{Z_{PS}}\right)\left(\frac{x}{Z_{PS}}\right)+\left(\frac{Y_{PS}}{Z_{PS}}\right)\left(\frac{y}{Z_{PS}}\right)\right]\right\} \tag{12}$$

The curly bracket in this expression depends only on the point on the planetary system that emits the radiation. It is the product of the strength of the point source at the point source location and the spherical wave evaluated at the origin of the interferometer-plane coordinate system. These are all constant quantities for a specific light emitting point on the celestial body in the planetary coordinate system, and its distance from the interferometer plane. See (Strojnik & Paez, 2001) for description of the Planckian radiators. Thus, they also form the constant amplitude of the wave at the interferometer plane, u_{PS0}.

$$u_{PS0}(X_{PS},Y_{PS},Z_{PS}) = u_{PS0}(0,0,0;X_{PS},Y_{PS},Z_{PS}) = U_{PS0}(X_{PS},Y_{PS},Z_{PS})\left[\frac{e^{ikr_{PS}(X_{PS},Y_{PS},Z_{PS})}}{r_{PS}(X_{PS},Y_{PS},Z_{PS})}\right]$$
$$= \left[\frac{U_{PS0}(X_{PS},Y_{PS},Z_{PS})}{r_{PS}(X_{PS},Y_{PS},Z_{PS})}\right]\exp[ikr_{PS}(X_{PS},Y_{PS},Z_{PS})] \tag{13}$$

We observe that the first factor is just amplitude, because all the quantities are constant. The second factor is an expression for the plane wave. We insert Eq. (13) into Eq. (12).

$$U_{PS}(x,y,z;X,Y,Z) = u_{PS0}(X_{PS},Y_{PS},Z_{PS})e^{-ikZ_{PS}\left[\left(\frac{X_{PS}}{Z_{PS}}\right)\left(\frac{x}{Z_{PS}}\right)+\left(\frac{Y_{PS}}{Z_{PS}}\right)\left(\frac{y}{Z_{PS}}\right)\right]}$$
$$= u_{PS0}(X_{PS},Y_{PS},Z_{PS})\exp\left\{-ikZ_{PS}\left[\left(\frac{X_{PS}}{Z_{PS}}\right)\left(\frac{x}{Z_{PS}}\right)+\left(\frac{Y_{PS}}{Z_{PS}}\right)\left(\frac{y}{Z_{PS}}\right)\right]\right\} \tag{14}$$

The first factor is just constant wave amplitude. The second factor is a plane wave, traveling in the direction along the z-axis, with a small tilt along the x- and y- direction.

Tilt depends on the source angular coordinates of the ($X_{PS}/Z_{PS} = \theta_{PSX}$, and $Y_{PS}/Z_{PS} = \theta_{PSY}$.

$$U_{PS}(x,y,z;X,Y,Z) = u_{PS0}(X_{PS},Y_{PS},Z_{PS})\exp\left[-ik(\theta_{PSx}x + \theta_{PSy}y) + \omega t + \delta\right] \tag{15}$$

The tilt of the plane wave in the x, y plane that originated at the Planetary system point X_{PS}, Y_{PS}, Z_{PS} depends on the coordinates of the point source. The tilt fringes are straight lines perpendicular to the tilt direction. For the point at the Planetary coordinate origin $X_{PS} = Y_{PS} = 0$, the plane wave travels along the Z-axis. Thus, only the central point on the Estrella generates plane wave radiation that produces no tilt.

We can form a significant general conclusion. The spherical waves originating at a point source at coordinates x_S, y_S, z_S of strength U_0 transform into a plane wave upon propagation over large distance r_S, with the amplitude reduced by the value of the spherical wave at distance r_S, {$\exp[ik(r_S)]/r_S$}, and the plane wave tilt equal to $\theta_x = x_S/z_S$ along the x-direction and $\theta_y = y_S/z_S$ in the y-direction, $\exp[ik(\theta_x x + \theta_y y)]$.

3.3 Two sources: the Estrella and the Tierra

We consider the case that both the Estrella and the Tierra are point sources, due to the small angles that they subtend at the aperture plane. The transformation of spherical waves originating at the Estrella and the Tierra into plane waves is illustrated in Fig. 8.

The radiometry allows for the point sources, establishing the concept of (spectral) intensity for such radiators (spectral power emitted per unit solid angle, $dP_\lambda/d\Omega$ [W/(sr µm)]. The coordinates X_E, Y_E, Z_E may assume some non-zero values, corresponding to the spatial extent of the star. Similarly, the Tierra is an extended body, about one tenth in diameter of the Estrella. Its coordinates may likewise assume the values corresponding to the extent of the Tierra. Figure 9 illustrates how an extended object may be perceived to emit the radiation from many small areas as point sources, and all transforming into plane waves.
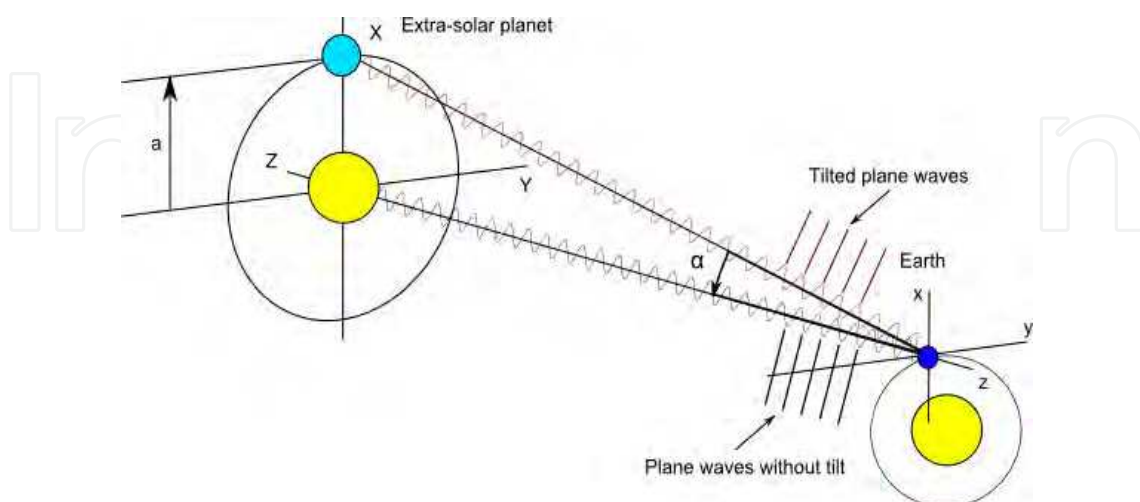

Fig. 8. The Estrella and the Tierra emit spherical waves. After free-space propagation, spherical waves become plane waves. They are tilted if they originate at an off-axis point, such as that on the Tierra.

3.4 Wave fronts from the Estrella and the Tierra incident on One aperture

The wave at the interferometer plane is the sum of those coming from the Estrella and the Tierra. We also include the temporal dependence associated with the traveling plane wave, ωt, to allow for the changes of the wave at a specific point in space as a function of time. We additionally include the phase delay δ. It may be used for temporal modulation.

$$
\begin{aligned}
u_{IP\lambda}(x,y,0;X,Y,Z) &= u_E(x,y,0;X_E,Y_E,Z_{PS}) + u_T(x,y,0;X_T,Y_T,Z_{PS}) \\
&= u_{E0}(X_E,Y_E,Z_{PS})\exp\left[-ik(\theta_{Ex}x + \theta_{Ey}y) + \omega t\right] \\
&\quad + u_{T0}(X_T,Y_T,Z_{PS})\exp\left[-ik(\theta_{Tx}x + \theta_{Ty}y) + \omega t + \delta\right]
\end{aligned}
\tag{16}
$$

At the interferometer plane (z=0), the wave from the Estrella and the wave from the Tierra add up. The coefficients for the amplitude correspond to the Estella and the Tierra as the point sources. Therefore, we drop the explicit spatial dependence on the coordinates to simplify the appearance of equations.

Two waves at the z = 0 interferometer plane produce incidance. It is found as the sum of the wave multiplied by its complex conjugate. (Spectral) incidance is defined in radiometry as power, incident per unit area (per unit wavelength) in [W/(m² μm)].

$$
\begin{aligned}
M_{AP}&(x,y,0;X,Y,Z) \\
&= \left[U_E(x,y,0;X_E,Y_E,Z_{PS}) + U_T(x,y,0;X_T,Y_T,Z_{PS})\right]\left[U_E(x,y,0;X_E,Y_E,Z_{PS}) + U_T(x,y,0;X_T,Y_T,Z_{PS})\right]^*
\end{aligned}
\tag{17}
$$

After substituting from Eq. (16), the incidance is found as a product of the sum of two traveling waves.

$$
\begin{aligned}
M_{AP}&(x,y,0;X,Y,Z) \\
&= \left\{u_{E0}(X_E,Y_E,Z_{PS})\exp\left[-ik(\theta_{Ex}x + \theta_{Ey}y) + \omega t\right] + u_{T0}(X_T,Y_T,Z_{PS})\exp\left[-ik(\theta_{Tx}x + \theta_{Ty}y) + \omega t + \delta\right]\right\} \\
&\quad \times \left\{u_{E0}(X_E,Y_E,Z_{PS})\exp\left[-ik(\theta_{Ex}x + \theta_{Ey}y) + \omega t\right] + u_{T0}(X_T,Y_T,Z_{PS})\exp\left[-ik(\theta_{Tx}x + \theta_{Ty}y) + \omega t + \delta\right]\right\}^*
\end{aligned}
\tag{18}
$$

Next, we change the signs of the complex exponents in the second line to implement the complex conjugate. We also omit the explicit dependence on the planetary system coordinates in the amplitude factors.

$$
\begin{aligned}
M_{IP\lambda}&(x,y,0;X,Y,Z) \\
&= \left\{u_{E0}\exp\left[-ik(\theta_{Ex}x + \theta_{Ex}y) + \omega t\right] + u_{T0}\exp\left[-ik(\theta_{Tx}x + \theta_{Ty}y) + \omega t + \delta\right]\right\} \\
&\quad \times \left\{u_{E0}^*\exp\left[+ik(\theta_{Ex}x + \theta_{Ex}y) - \omega t\right] + u_{T0}^*\exp\left[+ik(\theta_{Tx}x + \theta_{Ty}y) - \omega t - \delta\right]\right\}
\end{aligned}
\tag{19}
$$

We multiply the factors out to obtain a two-beam interference pattern in a complex form.

$$
\begin{aligned}
M_{IP\lambda}(x,y,0;X,Y,Z) &= u_{E0}u_{E0}^* + u_{T0}u_{T0}^* \\
&+ u_{E0}u_{T0}^*\exp\left\{-ik\left[(\theta_{Ex} - \theta_{Tx})x + (\theta_{Ey} - \theta_{Ty})y\right] - \delta\right\} + u_{E0}^*u_{T0}\exp\left\{+ik\left[(\theta_{Ex} - \theta_{Tx})x + (\theta_{Ex} - \theta_{Ty})y\right] + \delta\right\}
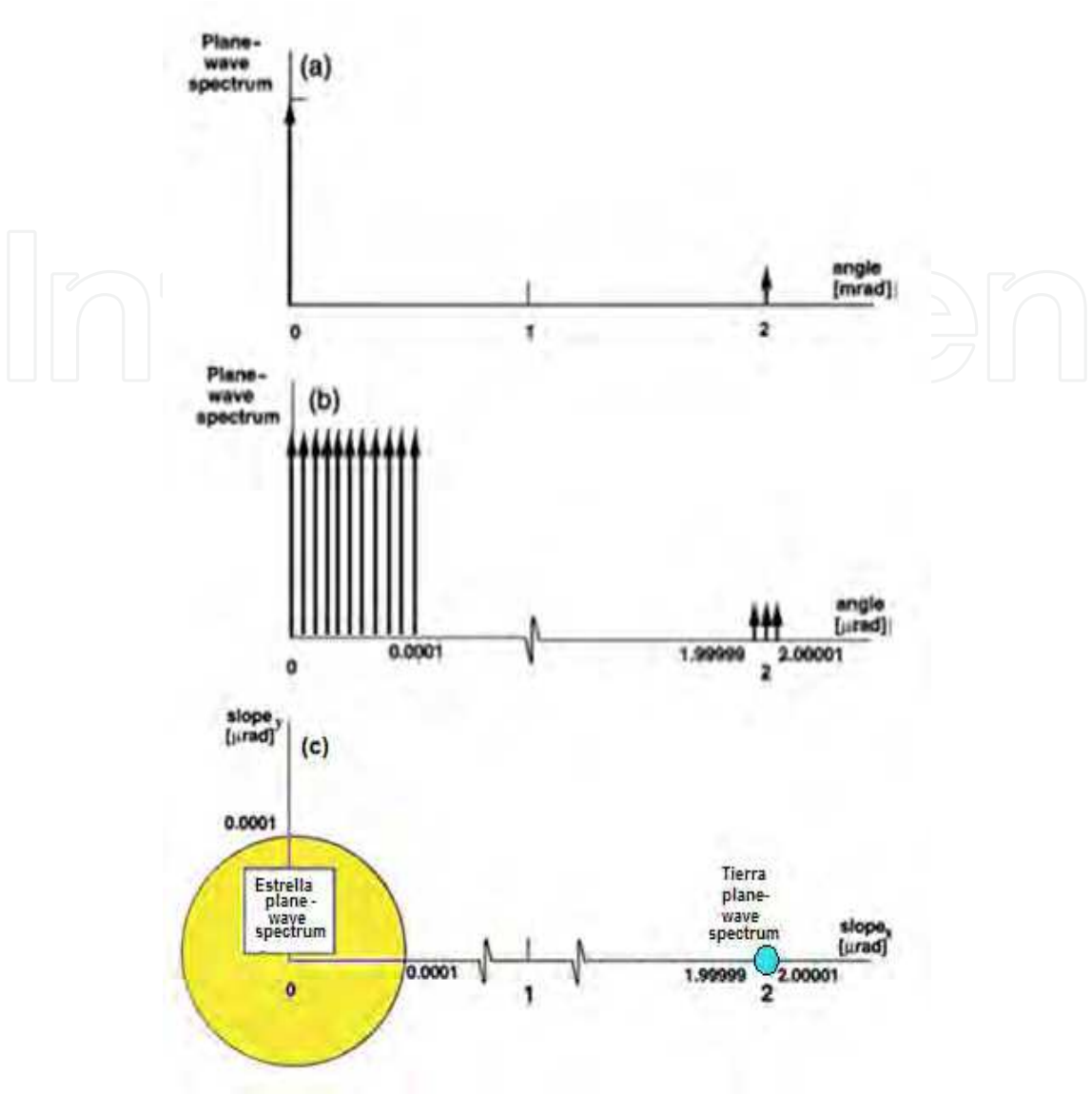\end{aligned}
\tag{20}
$$

Fig. 9. (a) The Estrella and the Tierra plane wave spectra as a function of angular coordinate. In the middle and the bottom diagrams (b) and (c), the angular coordinate shows discontinuity to allow the presentation of distinct plane waves with increasing inclination, both for the Estrella and for the Tierra. In the middle, the plane wave spectra are shown as a function of angle along which the Tierra is located. The bottom presentation exhibits the spectra as a function of x- and y- inclination, making explicit the symmetrical and asymmetrical features of the plane wave spectra. Those from the Tierra do not possess the cylindrical symmetry about the optical axis. Those from the Estrella exhibit cylindrical symmetry.

The complex numbers in the exponential form may be expanded as sine and cosine, according to the formula, [exp(+/-iα) = cosα +/- i sinα]. The sine terms cancel each other out, resulting in a (co)-sinosoidal modulation of the incidance, in addition to two incidances from the Estrella and the Tierra.

$$M_{IP\lambda}(x,y,0;X,Y,Z) = u_{E0}^2 + u_{T0}^2 + 2u_{E0}u_{T0}\cos\left\{\left(\frac{2\pi}{\lambda}\right)\left[\left(\theta_{Ex}-\theta_{Tx}\right)x + \left(\theta_{Ex}-\theta_{Ty}\right)y\right] + \delta\right\} \quad (21)$$

Using the trigonometric identity for a cosine of a double angle [$\cos(2\alpha) = 2\cos^2\alpha - 1$], we finally arrive at the expression for the interference of two un-equal beams. The incidance from two plane waves, slightly inclined with respect to each other exhibits straight fringes normal to the plane of the incident waves.

$$M_{AP}(x,y,0;X,Y,Z) = u_{E0}^2 - 2u_{E0}u_{T0} + u_{T0}^2 + 4u_{E0}u_{T0}\cos^2\left\{\left(\frac{\pi}{\lambda}\right)\left[(\theta_{Ex} - \theta_{Tx})x + (\theta_{Ey} - \theta_{Ty})y\right] + \partial\right\} \quad (22)$$

In absence of the Tierra, there is no radiation emitted from the Tierra. Therefore, there is no interference pattern, and Eq. (22) reduces to the first term. This is just the incidance from the Estrella. This is an important result, because the very detection of the interference fringes establishes the existence of the second point source, a companion Tierra. The phase delay term is halved. This is denoted by a different phase delay symbol in Eq. (22). The first three terms in Eq. (22) form a perfect square, so the expression for the incidance may be further simplified.

$$M_{AP}(x,y,0;X,Y,Z) = (u_{E0} - u_{T0})^2 + 4u_{E0}u_{T0}\cos^2\left\{\left(\frac{\pi}{\lambda}\right)\left[(\theta_{Ex} - \theta_{Tx})x + (\theta_{Ey} - \theta_{Ty})y\right] + \partial\right\} \quad (23)$$

The fringe direction is perpendicular to the orientation of the difference between the slopes of the plane waves coming from the respective points on the Estrella and the Tierra.

3.4.1 Modulation from the Estrella and the Tierra as point sources

Maximum incidance may be found fom Eq. (23) when the cosine square is equal to 1.

$$M_{AP\max}(x,y,0;X,Y,Z) = (u_{E0} + u_{T0})^2 \quad (24)$$

Cosine is one when the argument of the cosine-square function is an integral multiple of π.

$$\left(\frac{\pi}{\lambda}\right)\left[(\theta_{Ex} - \theta_{Tx})x + (\theta_{Ex} - \theta_{Ty})y\right] + \partial = N\pi \quad (25)$$

Minimum incidance may similarly be found when the cosine-square is equal to zero.

$$M_{AP\min}(x,y,0;X,Y,Z) = (u_{E0} - u_{T0})^2 \quad (26)$$

This condition is met when the argument of the cosine-square function is $\pi/2$, plus an integral multiple of π.

$$\left(\frac{\pi}{\lambda}\right)\left[(\theta_{Ex} - \theta_{Tx})x + (\theta_{Ex} - \theta_{Ty})y\right] + \partial = \pi\left(N + \frac{1}{2}\right) \quad (27)$$

Average incidance is then one-half of the sum of Eq. (24) and Eq. (26).

$$M_{APave}(x,y,0;X,Y,Z) = \left(\frac{1}{2}\right)\left\{\left[M_{AP\max}(x,y,0;X,Y,Z) + M_{AP\min}(x,y,0;X,Y,Z)\right]\right\}$$

$$= \left(\frac{1}{2}\right)\left[(u_{E0} + u_{T0})^2 + (u_{E0} - u_{T0})^2\right] = u_{E0}^2 + u_{T0}^2 \quad (28)$$

The average signal in the aperture plane is the square of the wave amplitude from the Estrella and the Tierra. Then, the modulation in incidence is the one-half of difference between Eq. (24) and (26).

$$
\begin{aligned}
M_{APamp}(x,y,0;X,Y,Z) &= \left(\frac{1}{2}\right)\left\{\left[M_{AP\max}(x,y,0;X,Y,Z) - M_{AP\min}(x,y,0;X,Y,Z)\right]\right\} \\
&= \left(\frac{1}{2}\right)\left[(u_{E0}+u_{T0})^2 - (u_{E0}-u_{T0})^2\right] = 2u_{E0}u_{T0} = 2\sqrt{M_{E0}M_{T0}}
\end{aligned}
\tag{29}
$$

The signal amplitude in the aperture plane is equal to twice the product of the wave amplitude from the Estrella and the Tierra. The amplitudes correspond to the square-root of the power quantities developed in the radiometric analysis of Section 2.

3.4.2 Fringe separation for the Estrella and the Tierra

The incidence maximum is achieved when the argument of the cosine-square function is equal to zero or is an integral multiple of π. Without loss of generality, we choose convenient parameters to assist in fringe evaluation.

$$
\theta_{Tx}x + \partial = N\lambda
\tag{30}
$$

Changing the integral number N by 1, we find the change in distance Δx corresponding to the fringe-to-fringe separation.

$$
\Delta x = \frac{\lambda}{\theta_{Tx}}
\tag{31}
$$

The delay factor just displaces the origin of fringes in the observation plane, so we momentarily set it aside. Then, with the Estrella at the origin, the Tierra in the orbit at 2 μrad, (2 x 10^{-6} rad), using the wavelength of about 300 microns, we evaluate Eq. (31) to be Δx = 150 m. This physically means that within the distance of 75 m, the incidence will change from its maximum value to its minimum value.

4. Instrument concept: Earth-based interferometer, with single-aperture telescope and 0.3 mm radiation

We propose to use a single large-diameter telescope to provide radiation from the Estrella and the Tierra to a Mach-Zehnder interferometer, illustrated in Fig. 10. The function of the telescope is to collect the radiation and generate a several-hundred times increase in the tilt of the incident plane waves from the Tierra. There is no change to the tilt of the Estrella radiation, incident parallel to the optical axis. Two detectors are used in quadrature to record the complementary interference patterns. Optical light path modulation in one arm of the interferometer assures the scanning of fringes with passing time. Constant incidence from the Estrella may be maximized at one detector and minimized at the other detector by the proper insertion of the optical path delay.

Large telescopes are currently available at atmospheric window at 0.3 mm. The simple Mach-Zehnder interferometer is easy to build and align. By employing a telescope system, the angle of incidence is magnified, and the fringe density is increased (Strojnik et al., 2007).

Optical components and detectors might represent the critical technology if it were not for the rapid technology development for the various space systems in the last 20 years.
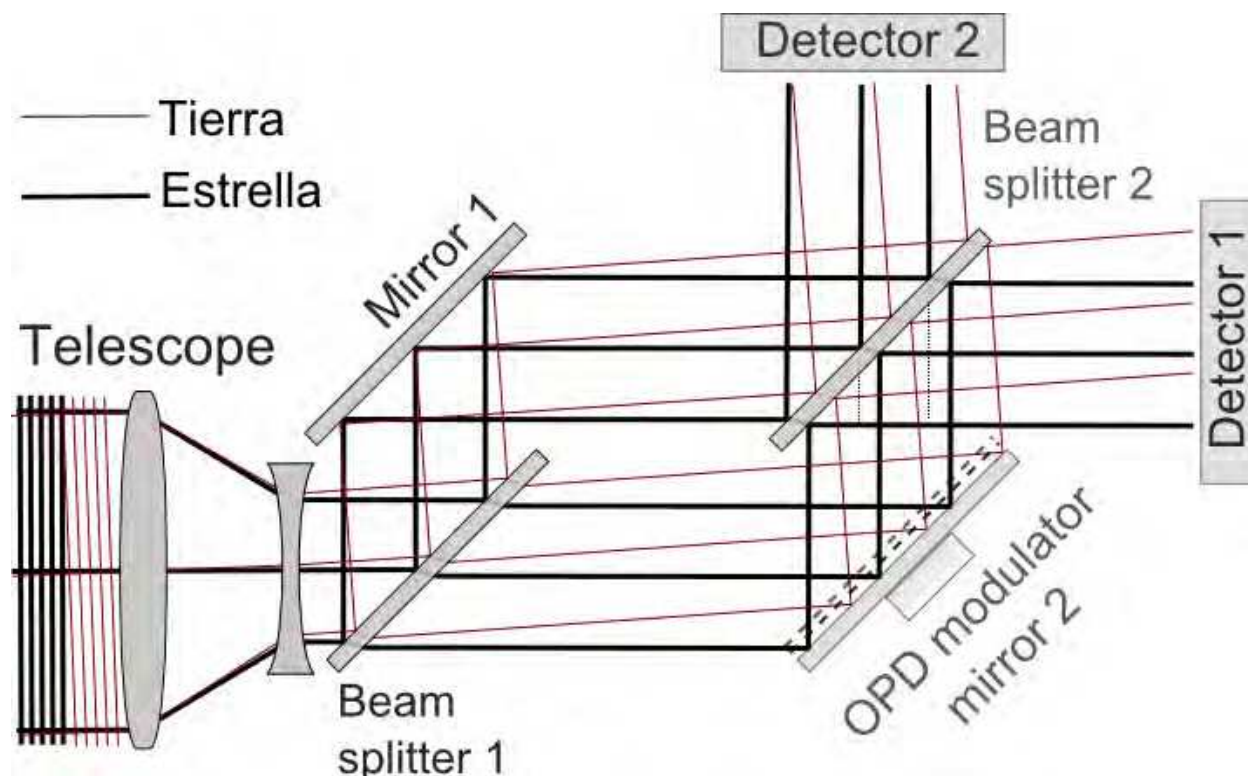

Fig. 10. A single large-diameter telescope provides radiation from the Estrella and the tilted wavefronts from the Tierra into a Mach-Zehnder interferometer. The primary function of the telescope is to collect the radiation. Its secondary function is to increase the angle of incidence of incomig tilted radiation. The radiation from the Estrella and from the Tierra passes through a beam splitter which sends part of each through a different interferometer arm. The optical path modulator (OPD) modulates the path in one arm of interferometer so that the light parallel to the optical axis, coming from the star, produces constructive and destructive interference on comnplimentary detectors. The tilted radiation keeps its angle of inclination and generates fringes.

5. Conclusions

We demonstrated theoretically that the existence of the Tierra is directly confirmed optically by detecting faint straight fringes, using a single aperture interferometer. The measured fringe separation at a given observation wavelength determines the angular separation of the Tierra from the center of the Estrella at the time of observation. If the observation continues for a number of Earth nights, the fringe separation will change slowly as the Tierra rotates about the Estrella. Furthermore, we developed the theoretical basis for the argument that the radiation from the Estrella is parallel to optical axis, while that coming from the Tierra has a tilt. We take advantage of the Tierra tilted waves in the proposed instrument design, where the tilt angle is multiplied using a single telescope aperture. Finally, we developed a new signal-to-noise ratio of 10^{-3} at a dramatically different wavelength from those studied previously. We propose to detect planets at 0.3 mm, where the Earth atmosphere is relatively transmissive, especially at high altitudes (0.4).

6. References

Agnese, P., Cigna, C., Pornin, J., Accomo, R., Bonnin, C., Colombel, N., Delcourt, M., Doumayrou, E., Lepennec, J., Martignac, J., Reveret, V., Rodriguez, L., & Vigroux, L. (2003). Filled Bolometer Arrays for Herschel/PACS. *Proceedings of SPIE 4855 Millimeter and Submillimeter Detectors for Astronomy*, Waikoloa, HI, USA, August 2002

Atacama large millimeter/submillimeter array, available from: https://almascience.nrao.edu/about-alma/weather/atmosphere-model [accessed 11/2/2011].

Arnold, G., Hiesinger, H., Helbert, J., Peter, G., & Walter, I. (2010). MERTIS−thermal IR imaging of Mercury: advances in mid-IR remote sensing technology for planetary exploration, *Proceeding of SPIE 7808 Infrared Remote Sensing and Instrumentation XVIII*, ISBN 9780819483041, San Diego, CA, USA, August 2010

Artamkin, A., Nikorici, A., Ryabova, L., Shklover, V., & Khokhlov, D (2006). Continuous focal plane array for detection of terahertz radiation, *Proceeding of SPIE 6297 Infrared Spaceborne Remote Sensing XIV*, ISBN 0-8194-6376-0, San Diego, CA, USA, August 2006

Becklin, E., & Gehrz, R. (2009). Stratospheric Observatory for Infrared Astronomy (SOFIA), *Proceeding of SPIE 7453 Infrared Spaceborne Remote Sensing and Instrumentation XVII*, ISBN 9780819477439, San Diego, CA, USA, August 2009

Beeman, J., & Haller, E. (2002). Far-infrared calibration sources for use in cryogenic telescopes, *Proceedings of SPIE 4486 Infrared Spaceborne Remote Sensing IX*, ISBN 0-8194-4200-3, San Diego, CA, USA, August 2001

Boeker, T., Lehmann, T., Storey, J., & Krabbe, A. (1997). MANIAC: a new mid- and near-infrared array camera, *Proceeding of SPIE 3122 Infrared Spaceborne Remote Sensing V*, ISBN 0-8194-2544-3, San Diego, CA, USA, July 1997

Bracewell, R. (1978). Detecting nonsolar planets by spinning infrared interferometer. *Nature* Vol. 274, (August 1978) pp. 780-781 ISSN 0028-0836

Brown, T., Charbonneau, D., Gilliland, L., Noyes, R., & Burrows, A. (2001). Hubble Space Telescope Time-Series Photometry of the Transiting Planet of HD 209458. *Astrophysical Journal*, Vol. 552, No. 2, (May 2001), pp. 699-709, ISSN 1538-4357

Butler, R., Bedding, T., Kjeldsen, H., McCarthy, C., O´Toole, S., Tinney, C., Marcy, G., & Wright, J. (2004). Ultra-High-Precision Velocity Measurements of Oscillations in AlphaCentauri A. *Astrophysical Journal*, Vol. 600, No. 1, (January 2001), pp. L75-L78, ISSN 1538-4357

Cageao, R., Alford, J., Johnson, D., Kratz, D., & Mlynczak, M. (2010). Far-IR measurements at Cerro Toco, Chile: FIRST, REFIR, and AERI, *Proceeding of SPIE 7808 Infrared Remote Sensing and Instrumentation XVIII*, ISBN 9780819483041, San Diego, CA, August 2010

CASU astronomical data centre, 2006. *The Hipparcos*. [online] Available at: http://archive.ast.cam.ac.uk/hipp/hipparcos.html, [Accessed 10/2/2011]

Catanzaro, B., Pham, T., Olmi, L., Martinson, K., & Devlin, M. (2002). Design and fabrication of a lightweight 2-m telescope for the balloon-borne large-aperture submillimeter telescope: BLAST, *Proceeding of SPIE 4818 Infrared Spaceborne Remote Sensing X*, ISBN 0-8194-4586-X, Seattle, WA, USA, July 2002

Diaz-Uribe, R., Campos-Garcia, M., & Granados-Agustin, F. (2002). Testing the optics of Large Millimeter Telescope (LMT), *Proceeding of SPIE 4818 Infrared Spaceborne Remote Sensing X*, ISBN 0-8194-4586-X, Seattle, WA, USA, July 2002

Elwell, J. (1993). SPIRIT II: a rocketborne interferometer spectrometer, *Proceedings of SPIE 2019 Infrared Spaceborne Remote Sensing*, ISBN 0-8194-1268-6, San Diego, CA, USA, July 1993

European Space Agency (2000-2011) Darwin: study ended no further activities planned, Available from http://www.esa.int/esaSC/120382_index_0_m.html, [accessed 11/2/2011].

European Space Agency (2000-2011).Planck at a glance ESA's microwave observatory Available from: http://www.esa.int/esaMI/Planck/SEMWN20YUFF_0.html, [accessed 10/30/2011].

Farhoomand, J., Yuen, L., Hoffman, A., Lum, N., Lum, L., & Young E. (2006). A 32x32 CTIA readout design for deep cryogenic applications, *Proceedings of SPIE 6297 Infrared Spaceborne Remote Sensing XIV*, ISBN 0-8194-6376-0, San Diego, CA, USA August 2006

Gordley, L., McHugh, M., Hervig, M., Burton, J., Liu, L., Magill, B., & Russell, J. (2005). Temperature, pressure and high-fidelity pointing knowledge for solar occultation using 2D focal plane arrays, *Proceedings of SPIE 5883 Infrared Spaceborne Remote Sensing*, ISBN 0-8194-5888-0, San Diego, CA, USA, August 2005

Hofferbert, R., Lemke, D., Groezinger, U., Henning, T., Mertin, S., Rohloff, R., Wagner, K., Wright, G., Visser, H., Katzer, J., Salvasohn, M., Posselt, W., Fargant, G., & Nalbandian, R. (2003). Cryomechanisms for the instruments MIRI and NIRSpec on the James Webb Space Telescope (JWST), *Proceeding of SPIE 5152 Infrared Spaceborne Remote Sensing XI*, ISBN 0-8194-5025-1, San Diego, CA, USA, August 2003

Hoogeveen, R., Yagoubov, P., Maurellis, A., Koshelets, V., Shitov, S., Mair, U., Krocka, M., Wagner, G., Birk, M., Huebers, H., Richter, H., Semenov, A., Goltsman, G., Voronov, B., & Ellison, B. (2003). New cryogenic heterodyne techniques applied in TELIS: the balloon-borne THz and submillimeter limb sounder for atmospheric research, *Proceeding of SPIE 5152 Infrared Spaceborne Remote Sensing XI*, ISBN 0-8194-5025-1, San Diego, CA, USA, August 2003

Hughes, D., Correa, J., Schloerb, F., Erickson, N., Romero, J., Heyer, M., Reynoso, D., Narayanan, G., Perez-Grovas, A., Souccar, K., Wilson, G., & Yun, M. (2010). The Large Millimeter Telescope, *Proceeding of SPIE 7733 Ground-based and Airborne Telescopes III*, ISBN 9780819482235 San Diego, CA, USA, July 2010

Krabbe, A., & Casey, S. (2002). First-light SOFIA instruments, *Proceeding of SPIE 4818 Infrared Spaceborne Remote Sensing X*, ISBN 0-8194-4586-X, Seattle, WA, USA, July 2002

Kelsall, T., Hauser, M., Berriman, G., Boggess, N., Moseley, S., Murdock, T., Silverberg, R., Spiesman, W., & Weiland, J. (1993). Investigation of the zodiacal light from 1 to 240 μm using COBE DIRBE data, *Proceeding of SPIE 2019 Infrared Spaceborne Remote Sensing*, ISBN 0-8194-1268-6, San Diego, CA, USA, July 1993

Kessler, M., & Harwit, M. (1993). Science with the Infrared Space Observatory, *Proceedings of SPIE 2019 Infrared Spaceborne Remote Sensing*, ISBN 0-8194-1268-6, San Diego, CA, USA, July 1993

Khokhlov, D., Galeeva, A. Dolzhenko, D., Ryabova, L., Nicorici, A., Ganichev, S., Danilov, S., & Belkov V. (2009). Photoconductive response of PbSnTe(In) in the terahertz spectral range, *Proceeding of SPIE 7453 Infrared Spaceborne Remote Sensing and Instrumentation XVII*, ISBN 9780819477439, San Diego, CA, USA, August 2009

Lamarre, J. (1993). FIRST (far-infrared and submillimeter space telescope): a major scientific project of ESA, *Proceeding of SPIE 2019 Infrared Spaceborne Remote Sensing*, ISBN 0-8194-1268-6, San Diego, CA, USA, July 1993

Large Millimeter Telescope Project. (1996-2006) Available from:

http://www.lmtgtm.org/telescope.html, [Accessed 10/25/2011].

http://www.lmtgtm.org/images/sitepics05012011/LMTatSunrise1.jpg, [Accessed 10/25/2011].

Latvakoski, H., Cardon, J., Larsen, M., & Elwell J. (2010). Pre-launch characterization of the WISE payload, *Proceedings of SPIE 7808 Infrared Remote Sensing and Instrumentation XVIII*, ISBN 9780819483041, San Diego, CA, USA, August 2010

Lemke, D., Groezinger, U., Hofferbert, R., Klaas, U., Boehm, A., & Rohloff R. (2005). Lessons learnt and implemented: from ISO- to HERSCHEL- and JWST-instrumentation, *Proceedings of SPIE 5883 Infrared Spaceborne Remote Sensing*, ISBN 0-8194-5888-0, San Diego, CA, USA, August 2005

Martijn, H., Gromov, A., Smuk, S., Malm, H., Asplund, C., Borglind, J., Becanovic, S., Alverbro, J., Halldin, U., Hirschauer, B. (2005). Far-IR linear detector array for DARWIN. *Infrared Phys. & Technol.*, Vol. 47, No. 1-2 (October 2005), pp. 106-114, ISSN 350-4495

Mather, C. (1993). Cosmic background explorer (COBE) mission, *Proceedings of SPIE 2019 Infrared Spaceborne Remote Sensing*, ISBN 0-8194-1268-6, San Diego, CA, USA, July 1993

Matsumoto, T., & Murakami, H. (1996). Infrared Telescope in Space (IRTS) mission, *Proceedings of SPIE 2817 Infrared Spaceborne Remote Sensing IV*, ISBN 0-8194-2205-3, Denver, CO, USA, August 1996

Maxey, C., Jones, C., Metcalfe, N., Catchpole, N., Gordon, N., White, A., & Elliot C. (1997). MOVPE growth of improved nonequilibium MCT device structures for near-ambient-temperature heterodyne detectors, *Proceedings of SPIE 3122 Infrared Spaceborne Remote Sensing V*, ISBN 0-8194-2544-3, San Diego, CA, USA, July 1997

Moutou, C., Mayor, M., Lo Curto, G., Ségransan, D., Udry, S., Bouchy, F., Benz, W., Lovis, C., Naef, D., Pepe, F., Queloz, D., Santos, N., & Sousa, S. (2011). The HARPS search for southern extra-solar planets XXVIII. Seven new planetary systems. *Astrophysical Journal*, Vol. 527, No. 2, (March 2001), pp. A63 ISSN 1538-4357

Müller, R., Gutschwager, B., Monte, C., Steiger, A., & Hollandt, J. (2010). Calibration of far-IR and sub-mm detectors traceable to the international system of units, *Proceedings of SPIE 7808 Infrared Remote Sensing and Instrumentation XVIII*, ISBN 9780819483041, San Diego, CA, USA, August 2010

NASA's Astrobiology Magazine 2007. *Catalog of Nearby Habitable Stars*. [online] Available at: http://www.nasa.gov/vision/universe/newworlds/HabStars.html, [Accessed 11/2/2011]

NASA's High Energy Astrophysics Science Archive Research Center, 2011. *Gliese Catalog of nearby Stars*. [online] Available at: http://heasarc.gsfc.nasa.gov/W3Browse/star-catalog/cns3.html, [Accessed 11/2/2011]

Olsen, C., Beeman, J., & Haller, E. (1997). Germanium far-infrared blocked impurity band detectors, *Proceeding of SPIE 3122 Infrared Spaceborne Remote Sensing V*, ISBN 0-8194-2544-3, San Diego, CA, USA, July 1997

Paez, G., & Strojnik, M. (2001). Telescopes In: *Handbook of Optical Engineering*, Malacara D., Thompson B., pp., 207-26, Marcel Dekker Inc., ISBN 0824746139, United Kingdom

Poglitsch, A., Waelkens, A., & Geis, N. (1999). Photoconductor array camera and spectrometer (PACS) for far-infrared and submillimetre telescope (FIRST), *Proceedings of SPIE 3759 Infrared Spaceborne Remote Sensing VII*, ISBN 0-8194-3245-8, Denver, CO, USA, July 1999

Reichertz, L., Cardozo, B., Beeman, J., Larsen, D., Tschanz, S., Jakob, G., Katterloher, R., Haegel, N., & Haller, E. (2005). First results on GaAs blocked impurity band (BIB)

structures for far-infrared detector arrays, *Proceedings of SPIE 5883 Infrared Spaceborne Remote Sensing*, ISBN 0-8194-5888-0, San Diego, CA, USA, August 2005

Richardson, L. (2007). A Spectrum of an Extrasolar Planet. *Nature* Vol 445 No 7130, (July 2007), pp. 892-895 ISSN 0028-0836

Royer, M., Fleury, J., Lorans, D., & Pelier A. (1997). Infrared detector development for the IASI instrument, *Proceeding of SPIE 3122 Infrared Spaceborne Remote Sensing V*, ISBN 0819425443, San Diego, CA, USA, July 1997

Schick, S., & Bell, G. (1997). Performance of the Spirit III cryogenic system, *Proceedings of SPIE 3122 Infrared Spaceborne Remote Sensing V*, ISBN 0-8194-2544-3, San Diego, CA, USA, July 1997

Scholl, M., & Paez, G. (1997a). Image-plane incidance for a baffled infrared telescope. *Infr. Phys. & Tech.*, Vol. 38, No. 2, (March 1997), pp. 87-92, ISSN 1350-4495

Scholl, M., & Paez, G. (1997b). Using the y, y-bar diagram to control stray light noise in IR systems. *Infr. Phys. & Tech.*, Vol. 38, No. 1, (February 1997), pp. 25-30, 1350-4495

Scholl, M. (1996a). Signal detection by an extra-solar-system planet detected by a rotating rotationally-shearing interferometer. *J. Opt. Soc. Am. A*, Vol. 13, No. 7 (July 1996), pp. 1584- 1592, ISSN 1084-7529

Scholl, M. (1996b). Design parameters for a two-mirror telescope for stray-light sensitive infrared applications. *Infr. Phys. & Tech.*, Vol. 37, No. 2, (March 1996), pp. 251 - 257, ISSN 1350-4495

Scholl, M. (1995). Star-Light Suppression with a rotating Rotationally-Shearing Interferometer for Extra-Solar Planet Detection in *Signal Recovery and Synthesis* Vol. 11 of 1995 OSA Technical Digest Series pp. 54–57 (Optical Society ofAmerica, Washington, D.C., 1995).

Scholl, M. (1994a). Rotating Interferometer for Detection and Reconstruction of Faint Objects – Simulation, *Proceeding of SPIE 2268 Infrared Spaceborne Remote Sensing II*, ISBN 0-8194-1592-8, San Diego, CA, USA, July 1994

Scholl, M. (1994b). Stray light issues for background-limited far-infrared telescope operation. *Opt. Eng.*, Vol. 33, No. 3, (March 1994), pp. 681-684, ISSN 0091-3286

Scholl, M. (1993). Apodization effects due to the size of a secondary mirror in a reflecting, on-axis telescope for detection of Extra-solar planets, *Proceedings of SPIE 2019 Infrared Spaceborne Remote Sensing*, ISBN 0-8194-1268-6, San Diego, California, July 1993

Scholl, M., & Eberlein S. (1993). Automated site characterization for robotic sample acquisition systems. *Opt. Eng.*, Vol. 32, No. 4, (April 1993), pp. 840-846, ISSN 0091-3286

Scholl, M. (1993). Experimental demonstration of a star field identification algorithm. *Opt. Lett.*, Vol.18, No. 6, (March 1993), pp. 412-404, ISSN 1539-4794

Schultz, A., Schroeder, D., Jordan, I., Bruhweiler, F., DiSanti, M., Hart, H., Hamilton, F., Hershey, F., Kochte, M., Miskey, C., Cheng, K., Rodrigue, M., Johnson, B., & Fadali S. (1999). Imaging planets about other stars with UMBRAS, *Proceedings of SPIE 3759 Infrared Spaceborne Remote Sensing VII*, ISBN 0-8194-3245-8, Denver, CO, USA, July 1999

Smithsonian Astrophysical Observatory, Telescope Data Center, 1991. *The Yale Bright Star Catalog, 5th revised edition*. [online] Available at: http://tdc-www.harvard.edu/catalogs/bsc5.html, [Accessed 10/2/ 2011]

Sofia Science Center, Stratospheric Observatory for Infrared Astronomy, Available from http://sofia.usra.edu/Science/instruments/waterVaporMonitor.html, [accessed 10/20/2011].

Stauder, J., & Esplin R. (1998). Stray light design and analysis of the Sounding of the Atmosphere using Broadband Emission Radiometry (SABER) telescope, *Proceedings of SPIE 3437 Infrared Spaceborne Remote Sensing VI*, ISBN 0-8194-2892-2, San Diego, California, July 1998

Strojnik, M., Paez, G., & Mantravadi M. (2007). Lateral Shearing Interferometry. In: *Optical Shop Testing*, Malacara D., pp. 649-700, Marcel Dekker Inc. ISBN 978-0-470-13596-9, New York

Strojnik, M., & Paez, G. (2003). Comparison of linear and rotationally shearing interferometric layouts for extrasolar planet detection from space. *Appl. Opt.*, Vol. 42, No.29, (October 2003) pp. 5897 – 5905, ISSN 2155-3165

Strojnik, M., & Paez, G. (2001). Radiometry, In: *Handbook of Optical Engineering*, Malacara D., Thompson B., pp. 649-700, Marcel Dekker Inc., ISBN 0824746139, United Kingdom

Suzuki, M., Kuze, A., Tanii, J., Villemaire, A., Murcray, F., & Kondo Y. (1997). Feasibility study on solar occultation with a compact FTIR, *Proceeding of SPIE 3122 Infrared Spaceborne Remote Sensing V*, ISBN 0-8194-2544-3, San Diego, CA, USA, July 1997

Thomas, P., Duggan, P., Pope, T., Sinclair, P., Soffer, R., Evstigneev, A., Zackodnick, N., & George M. (1998). Characteristics of a custom integrated bolometer array, *Proceeding of SPIE 3437 Infrared Spaceborne Remote Sensing VI*, ISBN 0-8194-2892-2, San Diego, CA, USA, July 1998

Touahri, D., Cameron, P., Evans, C., Haley, C., Osman, Z., Scott, A., & Rowlands, N. (2010). Tunable filter imager for JWST: etalon opto-mechanical design and test results, *Proceeding of SPIE 7808 Infrared Remote Sensing and Instrumentation XVIII*, ISBN 9780819483041, San Diego, CA, USA, August 2010

Udalski, A., Jaroszynski, M., Paczynski, B., Kubiak, M., Szymanski, M., Soszynski, I., Pietrzynski, G., Ulakzyk, K., Szewczyk, O., Wyrzykowski, L., Christie, G., DePoy, D., Dong, S., Gal-Yam, A., Gaudi, B., Gould, A., Han, C., Lepine, S., McCormick, J., Park, B., Pogge, R., Bennett, D., Bond, I., Muraki, Y., Tristram, P., Yock, P., Beaulieu, J., Bramich, D., Dieters, S., Greenhill, J., Hill, K., Horne, K., & Udalski, N. (2005). A Jovian Mass Planet in Microlensing Event OGLE-2005-BLG-071. *Astrophysical Journal*, Vol. 628, No. 2, (June 2005), pp. L109-L112, ISSN 1538-4357

Vazquez-Jaccaud, C., Strojnik, M., & Paez, G. (2010). Effects of a star as an extended body in extra-solar planet search. *Journal of Modern Optics*, Vol. 57, No.18- 20, (September 2009), pp. 1808–1814, ISSN 1362-3044

Wellard, S., Bingham, G., Latvakoski, H., Mlynczak, M., Johnson, D., & Jucks K. (2006). Far infrared spectroscopy of the troposphere (FIRST): flight performance and data processing, *Proceeding of SPIE 6297 Infrared Spaceborne Remote Sensing XIV*, ISBN 0-8194-6376-0, San Diego, CA, USA, August 2006

Wilson, G., Austermann, J., Logan, D., & Yun, M. (2004). First-generation continuum cameras for the Large Millimeter Telescope, *Proceeding of SPIE 5498 Millimeter and Submillimeter Detectors for Astronomy II,* Glasgow, SCO, UK, June 2004

Wright, J., Upadhyay, S., Marcy, G., Fischer, D., Ford, E., & Johnson, J. (2009). Ten new and updated multiplanet systems and survey of exoplanetary systems. *Astrophysical Journal*, Vol. 693, No. 2, (March 2001), pp. 1084-1089 ISSN 1538-4357 1362-3044

Wirtz, D., Sonnabend, G., & Schieder, R. (2003). THIS: next-generation infrared heterodyne spectrometer for remote sensing, *Proceeding of SPIE 5152 Infrared Spaceborne Remote Sensing XI*, ISBN 0-8194-5025-1, San Diego, CA, USA, August 2003

Young, E. (1993). Space infrared detectors from IRAS to SIRTF, *Proceedings of SPIE 2019 Infrared Spaceborne Remote Sensing*, ISBN 0-8194-1268-6, San Diego, CA, USA, July 1993
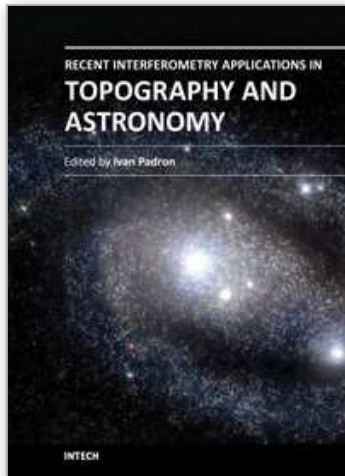
Recent Interferometry Applications in Topography and Astronomy

Edited by Dr Ivan Padron

This book provides a current overview of the theoretical and experimental aspects of some interferometry techniques applied to Topography and Astronomy. The first two chapters comprise interferometry techniques used for precise measurement of surface topography in engineering applications; while chapters three through eight are dedicated to interferometry applications related to Earth's topography. The last chapter is an application of interferometry in Astronomy, directed specifically to detection of planets outside our solar system. Each chapter offers an opportunity to expand the knowledge about interferometry techniques and encourage researchers in development of new interferometry applications.

How to reference

In order to correctly reference this scholarly work, feel free to copy and paste the following:

Marija Strojnik and Gonzalo Paez (2012). Interferometry to Detect Planets Outside Our Solar System, Recent Interferometry Applications in Topography and Astronomy, Dr Ivan Padron (Ed.), ISBN: 978-953-51-0404-9, InTech, Available from: http://www.intechopen.com/books/recent-interferometry-applications-in-topography-and-astronomy/interferometry-to-detect-planets-outside-our-solar-system

INTECH
open science | open minds